JOURNAL OF Applied Polymer SCIENCE

Peculiar Electrical and Photoelectric Behaviors in Conducting Multilayers: Insights into Accumulative Charge Tunneling

Min Wang, Qunwei Tang, Haiyan Chen, Benlin He
Institute of Materials Science and Engineering, Ocean University of China, Qingdao 266100, Shandong Province, People's Republic of China
Correspondence to: Q. Tang (E-mail: tangqunwei@hotmail.com) or H. Chen (E-mail: chen_hiyan@163.com)

ABSTRACT: Layer-by-layer self-assembly is a versatile technique for the construction of well-defined nanoarchitectures with outstanding electrical and photoelectric performances. The revelation of a potential charge-transfer mechanism of extraordinary electrical and photoelectric behaviors is profound in the design of modern electrical and photoelectrical devices. With the aim of revealing the potential charge-transfer mechanism in conducting multilayer films, in this study, we fabricated [poly(styrene sulfonate)/polyaniline]$_n$ [(PSS/PANi)$_n$] multilayers with peculiar electrical and photoelectrical features. The fantastic increments in sheet conductivity and photoelectric response were believed to be the percolation reflection of accumulative electrons tunneled across the insulating PSS from the bottom to the top of the conjugated structure of PANi. These profound phenomena, along with simple fabrication and a well-defined architecture, promise that the conducting multilayers will be good candidates for electronic and optoelectronic nanodevices. © 2013 Wiley Periodicals, Inc. J. Appl. Polym. Sci. **2014**, *131*, 40258.

KEYWORDS: membranes; nanostructured polymers; optical and photovoltaic applications; surfaces and interfaces

Received 30 October 2013; accepted 3 December 2013
DOI: 10.1002/app.40258

INTRODUCTION

A layer-by-layer (LbL) self-assembly technique is one of the most widely used approaches in the design of versatile and nanostructured ultrathin films for modern nanotechnology.[1–3] Among the diverse applications, nanodevices with extraordinary electrical and photoelectrical performances have been paid growing attention because of their potential utilization in energy-related fields.[4] Its merits of simplicity, universality, low-cost, and versatility in the combination of two or more distinct functional components into molecular-level architectures promote the LbL technique for applications in microelectronic manufacturing. Traditional approaches are limited in the fabrication of devices at the submicrometer level, which cannot provide satisfactory electrical, mechanical, optical, and photoelectrical behaviors. Therefore, the LbL technique opens a way for the exploration of extraordinary functions in nanofilms.

Studies in the field of LbL assembly have mushroomed in past decades; the overwhelming majority of them have been related to ultrathin films.[5–8] The pioneering work of Iler[9] in 1966 was not recognized until its rediscovery by Decher et al.[10,11] in the early 1990s. Since then, much progress has been achieved in some areas of technology, for instance, actuating, electronic materials, transport phenomena, and highlighted performances in mechanics. Free-standing polymeric films from LbL assembly are promising in the fabrication of actuators because of their rapid stimulus–response and flexibility. Humidoresponsive/thermoresponsive actuators have been successfully designed from poly(acrylic acid)/poly(allylamine hydrochloride) free-standing multilayer films and have shown quick and reversible bending–unbending motions at altered humidities and temperatures.[12] Conducting polymers are versatile electronic candidates with outstanding charge transports.[13,14] Conducting multilayer films originating from conducting polymers were assembled by a dipping LbL technique, and this resulted in a conductivity percolation phenomenon with bilayers.[15–19]

In the search for new performances of conducting multilayer films, we recently investigated the pertinent properties of [poly(-styrene sulfonate)/polyaniline]$_n$ [(PSS/PANi)$_n$] ultrathin films (n is the bilayer number). Here, we give insight into the electrical and photoelectric behaviors from the special perspective that they increased the charge-transport capacity with the reflection of a linearly increased conductivity and photocurrent density. The interesting multifunctional properties of the consolidated LbL films were demonstrated by electrochemical characterizations.

EXPERIMENTAL

Preparation of the Positively Charged PANi Solution

Polyaniline was synthesized by a chemical method with ammonium persulfate (APS) as an oxidant and hydrochloric acid (HCl)

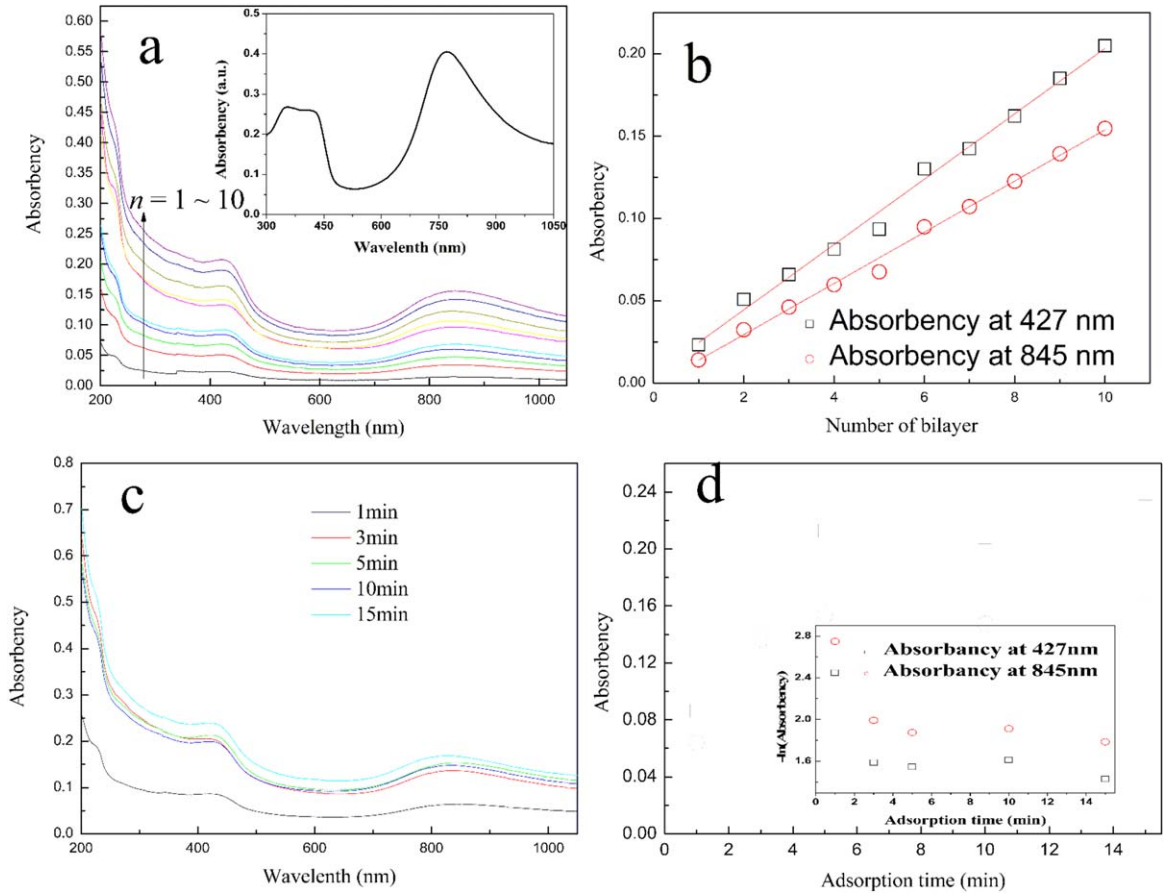

Figure 1. (a) UV–vis spectra of a $(PSS/PANi)_n$ multilayer within 10 bilayers. The insert is the UV–vis spectrum of a PANi aqueous solution. (b) Linear plots of the absorbance intensity of PANi as a function of the bilayer number. (c) UV–vis spectra of $(PSS/PANi)_5$ with various deposition times. (d) Plots of the intensity of the PANi absorbance as a function of the deposition time in the $(PSS/PANi)_5$ multilayers. The insert is a plot of $-\ln A$ versus the adsorption time of PANi. [Color figure can be viewed in the online issue, which is available at wileyonlinelibrary.com.]

as a doping agent. Under magnetic stirring, an aqueous solution of APS was slowly dropped into a solution composed of 1 mL of aniline monomer (the molar ratio of APS to aniline monomer was 1:1) and 1 m*M* HCl aqueous solution. With polymerization of the mixture sustained for 30 min at room temperature, the reactant was placed at 0°C for 12 h to obtain a very soluble PANi. After pump filtration, deionized water washing, and vacuum drying at 50°C, anhydrous PANi powders were obtained and were subsequently prepared for a 0.5*M* aqueous solution (pH ≈ 2.5).

Assembly of the $(PSS/PANi)_n$ Ultrathin Films

LbL assembly of the $(PSS/PANi)_n$ ultrathin films was carried out on cleaned glass substrates. Before the LbL assembly, the glass slide was cleaned with piranha solution (7:3 v/v concentrated H_2SO_4/H_2O_2) for 1 h; this was followed by thorough rinsing with deionized water, anhydrous ethanol, and deionized water again. For the LbL assembly, the clean glass slide was immersed in a PANi aqueous solution for 5 min, rinsed with deionized water for 1 min, and dried by an N_2 gas stream. Then, it was immersed in a 1 m*M* PSS aqueous solution for 5 min, rinsed again for 1 min, and dried by an N_2 gas stream. We obtained $(PSS/PANi)_n$ films with various bilayer numbers by repeating the cycles.

Electrochemical Characterization

We evaluated the electrical behaviors by recording the alternating-current impedance spectroscopy on a CHI660E electrochemical workstation in a frequency range of 0.1 Hz to 1 MHz and an alternating-current amplitude of 0 mV at room temperature in a 0.5*M* H_2SO_4 solution. Glassy carbon pole (diameter = 5 mm) coated $(PSS/PANi)_n$ films were used as working electrodes, a Pt sheet with a size of $1 \times 1 \times 0.3$ cm^3 was the counter electrode, and Ag/AgCl was the reference electrode. The ohmic resistance associated with the film was determined from high-frequency intersection of the spectrum with the Z' (real axis) axis, from which the conductivity could be calculated on the basis of dimensional information. Cyclic voltammetry (CV) was also conducted on the same equipment. Before the measurement, the electrolyte was deoxygenated by nitrogen bubbling for 5 min.

Photoelectronic Tests

To record the photoelectronic performances of the resulting $(PSS/PANi)_n$ multilayers, the films were assembly on an fluorine doped tin oxide (FTO) glass substrate (12 Ω·cm^2). Before assembly, the FTO glass substrate was ultrasonically treated in deionized water for 15 min, acetone/H_2O (v/v = 1/1) for 15 min, and ethanol for 15 min and was again deionized water for

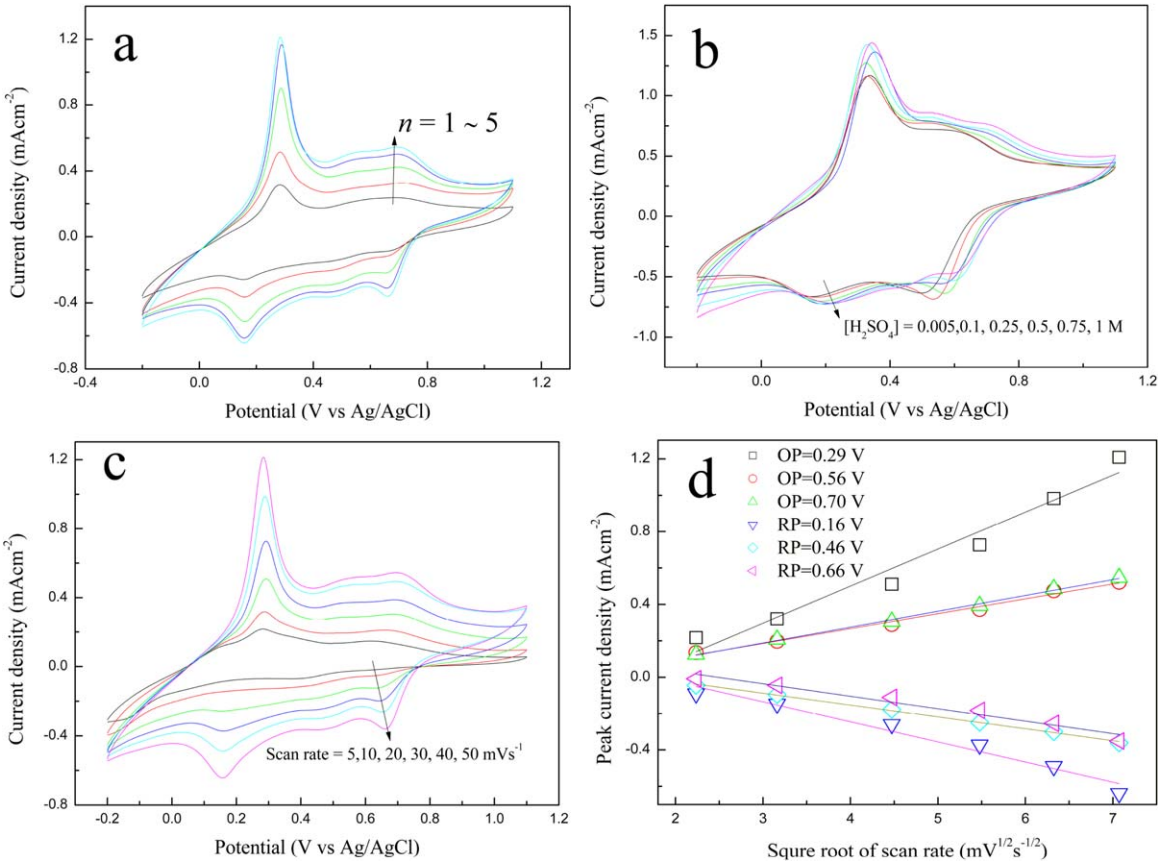

Figure 2. (a) CV curves of the $(PSS/PANi)_n$ multilayer films in 0.5*M* H_2SO_4 aqueous solutions recorded at a scan rate of 0.05 V/s. (b) CV curves of the $(PSS/PANi)_{10}$ multilayer films in H_2SO_4 aqueous solutions of various concentrations recorded at a scan rate of 0.05 V/s. (c) CV curves of the $(PSS/PANi)_5$ multilayer films in 0.5*M* H_2SO_4 aqueous solutions recorded at various scan rates. (d) Linear plots of the redox peak current density as a function of $(\text{scan rate})^{1/2}$. OP and RP represent oxidation peak and reduction peak, respectively. [Color figure can be viewed in the online issue, which is available at wileyonlinelibrary.com.]

15 min. The cleaned FTO glass slide was dried by an N_2 gas stream and was immersed in concentrated H_2SO_4/H_2O_2 (7:3 v/v) for 24 h and was subsequently dried by an N_2 gas stream. The pretreated substrate was immersed in PANi and PSS aqueous solutions alternatively; this was opposite to the method used in the glass substrate. Photoelectronic testing was carried out on a CHI660E electrochemical workstation with FTO-glass-supported $(PSS/PANi)_n$ films, a Pt sheet, and Ag/AgCl as the working electrode, counter electrode, and reference electrode, respectively. All of the measurement were tested in a rectangular quartz vessel with a size of 5 × 5 × 7 cm^3. The thickness of the wall was 2.5 mm. The photocurrent density versus time curves were recorded in the dark and with irradiation of simulated sunlight (100 mW/cm^2) from a 500 W Xe lamp (CHF-XM-500 W).

Other Characterizations

Ultraviolet–visible (UV–vis) absorption measurements were taken with a Mapada 3200 UV–vis spectrometer.

RESULTS AND DISCUSSION

UV–vis absorption spectroscopy was used to gain further insight into the assembly mode of the $(PSS/PANi)_n$ film [Figure 1(a)]. Three characteristic bands were detected in the UV–vis spectra: a shoulder band around 225 nm was attributed to the absorption of PSS, whereas the maximum bands at 427 and 845 nm were attributed to $\pi \rightarrow$ localized polaron band of PANi. The appearance of these two bands indicated that PANi was in its emeraldine state.[20] The increase in absorbance was attributed to the continuous absorption of the PANi and PSS layer. The absorbances at 427 and 845 nm increased linearly with the bilayer number [Figure 1(b)]; this indicated that the same amounts of PSS and PANi were deposited in each dipping cycle, and the multilayer was formed in a regular manner.[21] The self-assembly of the multilayers depended on the adsorption time, as shown in Figure 1(c). As the adsorption time increased from 0.5 to 5 min, the absorbances of the PSS/PANi bilayer at 427 and 845 nm increased sharply until they reached maxima at 5 min, as shown in Figure 1(d); this indicated that dense, homogeneous multilayers were assembled. Plots of $-\ln A$ versus adsorption time are shown in the insert (*A* is absorbency). Poor linear correlation was observed; this suggested that the adsorption of PANi obeyed higher order kinetics (second or third).[22]

CV was performed after each assembly of PSS and PANi. Figure 2(a) shows the CV of a glassy carbon pole coated with $(PSS/PANi)_n$ multilayers in a 0.5*M* H_2SO_4 aqueous solution.

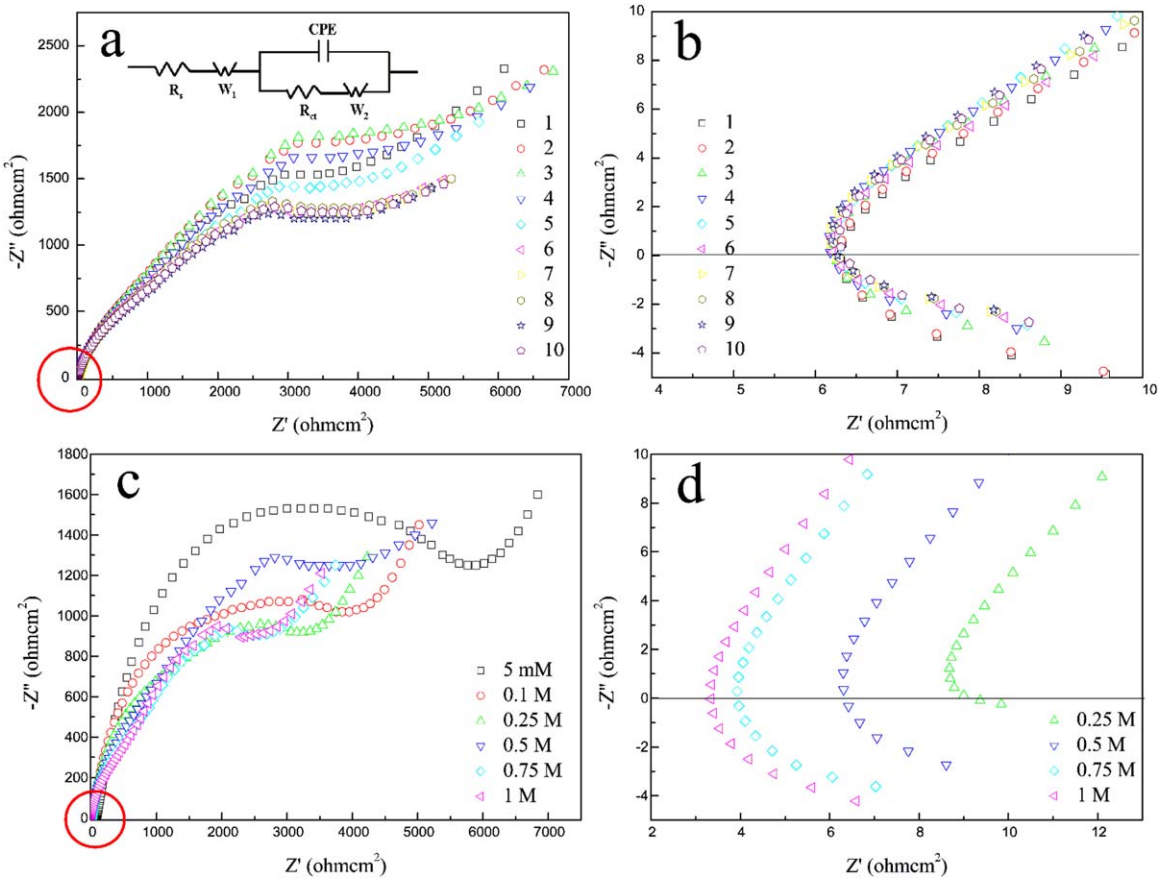

Figure 3. (a,b) Experimental EIS spectra for the glassy-carbon-electrode-supported $(PSS/PANi)_n$ multilayers ($n = 1$–10) in 0.5*M* H_2SO_4 aqueous solutions. (c,d) Experimental EIS spectra for the glassy-carbon-electrode-supported $(PSS/PANi)_{10}$ multilayers in H_2SO_4 aqueous solution of various concentrations. *Z″* is imaginary axis, W_1 is Warburg impedance. [Color figure can be viewed in the online issue, which is available at wileyonlinelibrary.com.]

Very reversible broad redox waves were recorded at about 0.5 and ~0.3 V; these corresponded to the redox reaction of oxygen species on PANi and indicated that PANi was assembled into the multilayer. The redox current densities were estimated, and plots of the current densities versus the number of bilayers are shown in insert. A linear increase in the current densities with bilayers was observed; this further confirmed that a similar amount of PANi was adsorbed for each assembly. From the redox reaction $PANi^+Cl^- + e + H^+ \rightarrow PANi^0 + (H^+Cl^-)$, we observed that protons from H_2SO_4 participated in the reduction of $PANi^+$ to $PANi^0$ and the oxidation of $PANi^0$ to $PANi^+$. A higher proton concentration was facile for accelerating the redox reaction between $PANi^+$ and $PANi^0$. Therefore, the CV curves recorded in the H_2SO_4 solution with higher concentration gave higher peak current densities, as shown in Figure 2(b). A sensitive criterion for determining the charge-transfer mechanism is the recording of the CV curves at various scan rates [Figure 2(c)], with peak current densities plotted against the square roots of the scan rates for the PSS/PANi multilayer. The linearity of the peak current densities with the square root of the scan rates in Figure 2(d) indicated that charge transfer in the redox step was controlled by the diffusion of charges in the films, as described by the empirical Randles–Sevcik theory:[23]

$$i_p = (2.69\times10^5) n^{3/2} A D_{ct}^{1/2} \nu^{1/2} C_0 \quad (1)$$

where i_p is peak current density, $\nu^{1/2}$ is square root of scan rate, D_{ct} is the charge-transport diffusion coefficient and C_0 is the concentration of electroactive sites. The dependence of the peak current densities on scan rate is determined by $D_{ct}\tau/d^2$, where τ is the experimental timescale (the time for the potential to traverse the wave) and d is the film thickness. $D_{ct}\tau/d^2 \gg 1$ means that the charger-transfer rate is significantly high compared to the experimental time and gives a linear fitting of the peak current density versus the scan rate. However, the peak current density is directly proportional to the square root of the scan rate at $D_{ct}\tau/d^2 \ll 1$; this gives a much smaller charge-transfer rate.

Electrochemical impedance spectrum (EIS) was successfully used to characterize the formation and intrinsic charge-transfer of the PSS/PANi multilayer. R_s describes the resistance of the inside and outside of a thin film (i.e., film resistance), R_{ct} is provided by the electrochemical double layer at the interface. W_1 reflects the diffuse resistance of ions inside the multilayers, and CPE is a constant phase element, a reflection of surface area of a film, which is frequently used as a substitute for the capacitor in an equivalent circuit to fit the impedance behavior of the electrical double layer more accurately when the double layer does not behave as an ideal capacitor. As illustrated in Figure 3, the EIS data fit well with the

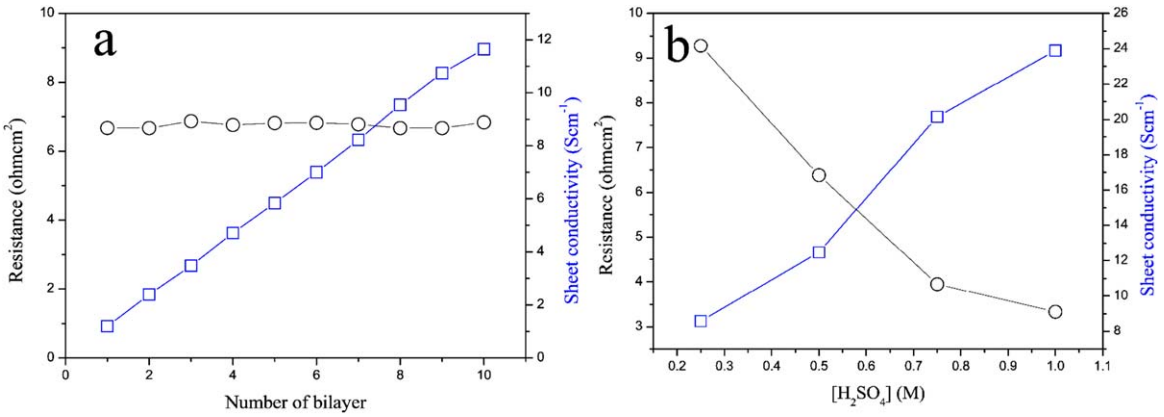

Figure 4. (a) Plots of the electrical resistance and sheet conductivity of the $(PSS/PANi)_n$ multilayers as a function of the bilayer number in 0.5*M* H_2SO_4 aqueous solutions. (b) Plots of the electrical resistance and sheet conductivity of the $(PSS/PANi)_n$ multilayers as a function of the H_2SO_4 concentration. [Color figure can be viewed in the online issue, which is available at wileyonlinelibrary.com.]

curves and gave an equivalent circle, as shown in Figure 3. There was a characteristic in which R_s was an approximate constant instead of depending on the bilayer number. However, the film thickness grew in a linear manner; therefore, the electrical conductivity of the multialayer had an increasing linear correlation with the bilayer number, as shown in Figure 4.

The electron tunneling effect is of significance in clarifying the conductivity of conducting composites by the integration of an insulator polymer with conductive fillers.[24–26] We believed that the electron tunneling effect was also applicable to the $(PSS/PANi)_n$ multilayer, where electron tunneling from the bottom PANi layer to the upper PANi layer across the insulating PSS was caused by the voltage on the multilayer. Electron tunneling always occurs in composites with a distance of conducting component to the conducting component in several to hundreds of nanometers. The tunneling assisted charges are expressed as follow:[27]

$$Q \propto \exp(-Ad) \tag{2}$$

where Q is charge, A and d represent the tunnel parameter and tunnel distance, respectively. A higher d indicated that the electron tunneling across the insulating PSS met with higher resistance. Moreover, the well-defined structure between the conducting and insulating phases allowed a robust electron tunneling and, therefore, increased accumulative charges on the upper PANi layer. It has been known that the self-assembled multilayer films are honored as highly ordered multilayer architecture, and the schematic diagram of electron tunneling within the $(PSS/PANi)_n$ multilayer is shown in Figure 5. Positively charged PANi of several nanometers was adsorbed on the negatively charged FTO substrate with the stacking of negatively charged PANi on PSS. In sequence, conducting multilayers with alternating PSS and PANi could be fabricated, in which PANi was believed to be parallel to the FTO substrate because of its negative charge configuration and the ordering nature of the self-assembly technique. Electron tunneling occurred in the conjugated structure of PANi. The electrical behaviors of the

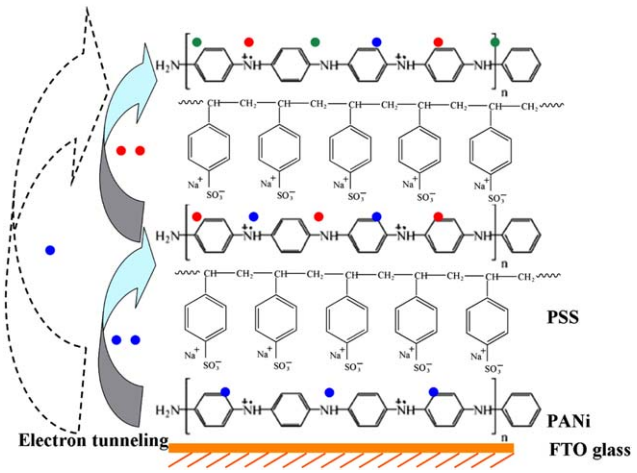

Figure 5. Proposed schematic diagram for electron tunneling within a $(PSS/PANi)_n$ multilayer. [Color figure can be viewed in the online issue, which is available at wileyonlinelibrary.com.]

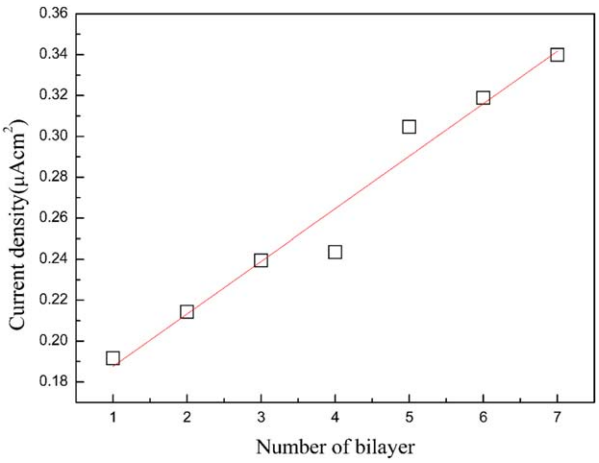

Figure 6. Transient photocurrent responses of the $(PSS/PANi)_n$ multilayers with various bilayer numbers (n = 1–7) under the irradiation of simulated sunlight (100 mW/cm^2). [Color figure can be viewed in the online issue, which is available at wileyonlinelibrary.com.]

$(PSS/PANi)_n$ multilayer was the reflection of accumulated charges on the PANi layer. As depicted in Figure 5, the charges on the first PANi layer were believed to be from the intrinsic PANi itself; however, the charge transfer on the top PANi layer was an accumulated effect of electrons from itself and tunneled electrons from the bottom PANi layers. From the linear increase in the conductivity, we concluded that there may have been a linear charge accumulation with increasing bilayers. The extraordinary electron tunneling effect was expected to give remarkable electrical and photoelectrical behaviors.

Photocurrent responses of the $(PSS/PANi)_n$ multilayers with varied bilayer numbers ($n = 1–7$) were probed to assess the dependence of accumulative photogenerated charges on the graphene oxide layers. Figure 6 shows that the photocurrent responses of the $(PSS/PANi)_n$ multilayers were highly dependent on the deposition cycles of PANi, in which the photocurrent of the conducting films exhibited an increasing intensity with deposition cycle. This indicated that the photogenerated electrons also had a tunneling effect from the bottom to the top of the PANi layers and gave an enhanced photocurrent density. The tunneling mechanism was similar to that of electrical conductivity because of a linear increase in the photocurrent density with the number of bilayers. The linear increase in accumulative charges significantly should promote their application in conducting multilayer films in photovoltaic cells, photocatalysts, batteries, and supercapacitors.

CONCLUSIONS

In summary, we demonstrated the fabrication of conducting $(PSS/PANi)_n$ multilayer films via a LbL technique. The uniform deposition process of the multilayer obeyed higher order kinetics. The $(PSS/PANi)_n$ multilayer gave a linear increase in conductivity; this was a reflection of accumulative charges on PANi. The electron tunneling mode is a potential mechanism for disclosing linearly the increased charge quantity from the bottom to the top of the PANi layer across the insulating PSS layer. A similar phenomenon also occurred in the photocurrent response. These fancy behaviors, along with the profound advantages of easy synthesis and versatile electrical and photoelectric performances promise that the conducting multilayers will be excellent electrode materials in photovoltaic cells, photocatalysts, batteries, and supercapacitors.

ACKNOWLEDGMENTS

The authors gratefully acknowledge Ocean University of China for providing a seed fund for this project and the Fundamental Research Funds for the Central Universities (contract grant numbers 201313001 and 201312005), the Shandong Province Outstanding Youth Scientist Foundation Plan (contract grant number BS2013CL015), the Doctoral Fund of the Ministry of Education of China (contract grant number 20130132120023), the Shandong Provincial Natural Science Foundation (contract grant number ZR2011BQ017), and the Research Project for the Application Foundation in Qingdao (contract grant number 13-1-4-198-jch).

REFERENCES

1. Govindaraju, T.; Avinash, M. B. *Nanoscale* **2012**, *4*, 6102.
2. Jaiswal, A.; Colins, J.; Agricole, B.; Delhaes, P.; Ravaine, S. *J. Colloid Interface Sci.* **2003**, *261*, 330.
3. Tang, Q. W.; Li, Q. H.; Lin, J. M.; Fan, S. J.; Hu, D.; Wu, J. H. *Polym. Compos.* **2010**, *31*, 145.
4. Reiss, P.; Couderc, E.; Girolamo, J. D.; Pron, A. *Nanoscale* **2011**, *3*, 446.
5. Cassagneau, T.; Guerin, F.; Fendler, J. H. *Langmuir* **2000**, *16*, 7318.
6. Sun, J. Q.; Wu, T.; Liu, F.; Wang, Z. Q.; Zhang, X.; Shen, J. C. *Langmuir* **2000**, *16*, 4620.
7. Adamczyk, Z.; Weronski, P.; Barbasz, J. *J. Colloid Interface Sci.* **2008**, *317*, 1.
8. Tang, Q. W.; Wu, J. H.; Li, Q. H.; Lin, J. M. *Polymer* **2008**, *49*, 5329.
9. Iler, R. K. *J. Colloid Interface Sci.* **1966**, *21*, 569.
10. Decher, G. *Science* **1997**, *277*, 1232.
11. Decher, G.; Hong, J. D.; Schmitt, J. *Makromol. Chem. Macromol. Symp.* **1991**, *46*, 321.
12. Ma, Y.; Sun, J. *Chem. Mater.* **2009**, *21*, 898.
13. Ma, Y.; Zhang, J.; Zhang, G.; He, H. *J. Am. Chem. Soc.* **2004**, *126*, 7097.
14. Cui, P.; Seo, S.; Lee, J.; Wang, L.; Lee, E.; Min, M.; Lee, H. *ACS Nano* **2011**, *5*, 6826.
15. Tang, Q. W.; Tang, Z. Y.; Wu, J. H.; Lin, J. M. *J. Mater. Chem.* **2011**, *21*, 5378.
16. Wu, J. H.; Tang, Q. W.; Sun, H.; Lin, J. M.; Ao, H. Y.; Huang, M. L.; Huang, Y. F. *Langmuir* **2008**, *24*, 4800.
17. Cheung, J. H.; Stockton, W. B.; Rubner, M. F. *Macromolecules* **1997**, *30*, 2712.
18. Kumar, B.; Park, Y. T.; Castro, M.; Grunlan, J. C.; Feller, J. F. *Talanta* **2012**, *88*, 396.
19. Tang, Q. W.; Wu, J. H.; Sun, X. M.; Li, Q. H.; Lin, J. M. *J. Colloid Interface Sci.* **2009**, *337*, 155.
20. Tang, Q. W.; Wu, J. H.; Sun, X. M.; Li, Q. H.; Lin, J. M. *Langmuir* **2009**, *25*, 5253.
21. Moriguchi, I.; Teraoka, Y.; Kagawa, S.; Fendler, J. H. *Chem. Mater.* **1999**, *11*, 1603.
22. Suib, S. L.; Segal, S. R. *Chem. Mater.* **1997**, *9*, 2526.
23. Xiao, Y. M.; Lin, J. Y.; Tai, S. Y.; Chou, S. W.; Yue, G. T.; Wu, J. H. *J. Mater. Chem.* **2012**, 22, 19919.
24. Hermant, M. C.; van der Schoot, P.; Klumperman, B.; Koning, C. E. *ACS Nano* **2010**, *4*, 2242.
25. Watts, P. C. P.; Hsu, W. K.; Kroto, H. W.; Walton, D. R. M. *Nano Lett.* **2003**, *3*, 549.
26. Zeng, X.; Xu, X. P.; Shenai, M.; Kovalev, E.; Baudot, C.; Mathews, N.; Zhao, Y. *J. Phys. Chem. C* **2011**, *115*, 21685.
27. Shrivastava, N. K.; Suin, S.; Maiti, S.; Khatua, B. B. *Ind. Eng. Chem. Res.* **2013**, *52*, 2858.